Supporting Information for

A bismuth ferrite-based lead-free piezoelectric ceramic surpassing PZT-8 in thermal stability

Xiaodong Yan[1], Chaoyang Shi[2], Jianjun Wu[3], Kevin Chen[4*], Zhengbao Yang[1*]

[1]Department of Mechanical and Aerospace Engineering, The Hong Kong University of Science and Technology, Clear Water Bay, Hong Kong, China
[2]School of Mechanical Engineering, Tianjin University, Tianjin, 300072, China
[3]Sichuan Energy Investment Tianfu Clean Energy Research Institute, Chengdu, 610041, China
[4]Department of Electronic and Computer Engineering, The Hong Kong University of Science and Technology, Clear Water Bay, Hong Kong, China

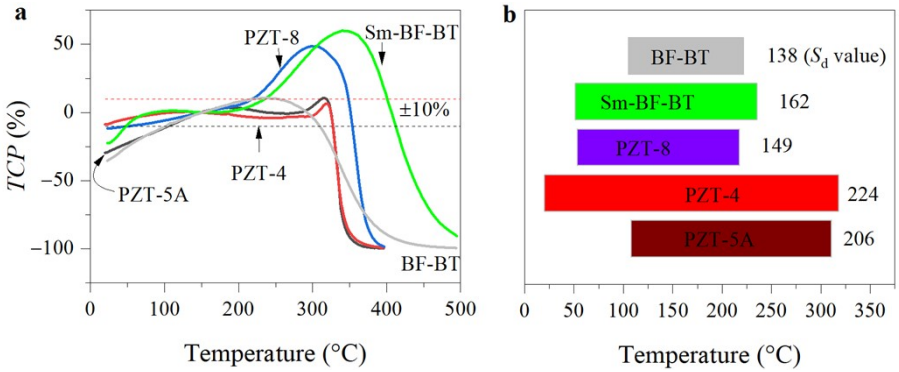

Fig. S1. **a**, The temperature coefficient, **b**, Temperature-stable range and thermal stability metric S_d of d_{33} of the five types of materials based on the ±10% threshold, the benchmark is 150 °C.

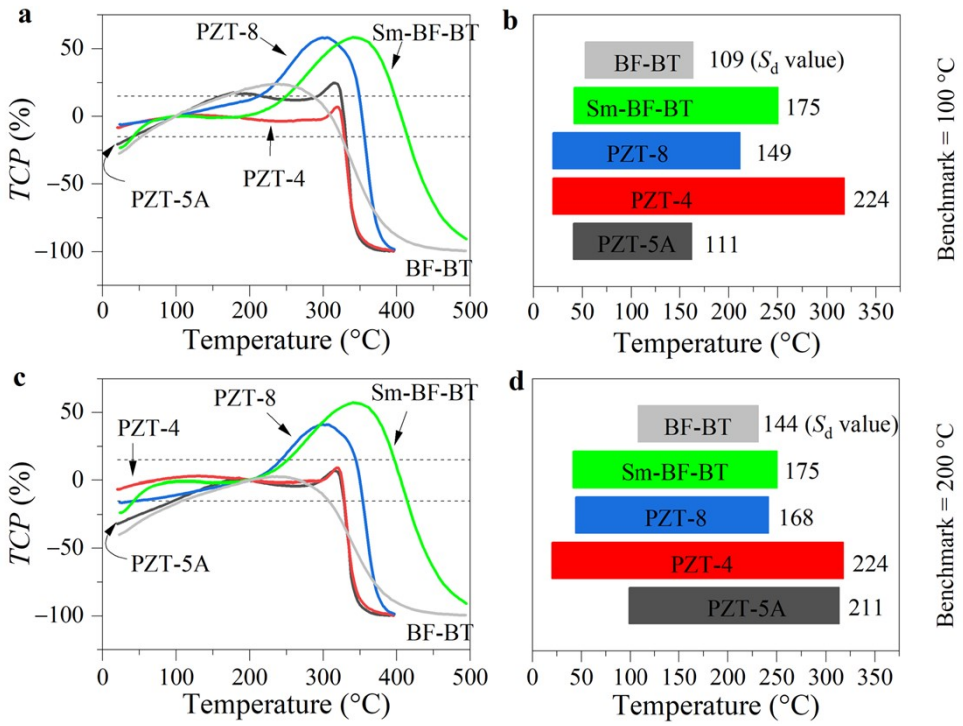

Fig. S2. The temperature coefficient, temperature-stable range and thermal stability metric S_d of d_{33} of the five types of materials based on the benchmark of 100 °C (**a** and **b**) and 200 °C (**c** and **d**), the threshold is ±15%.

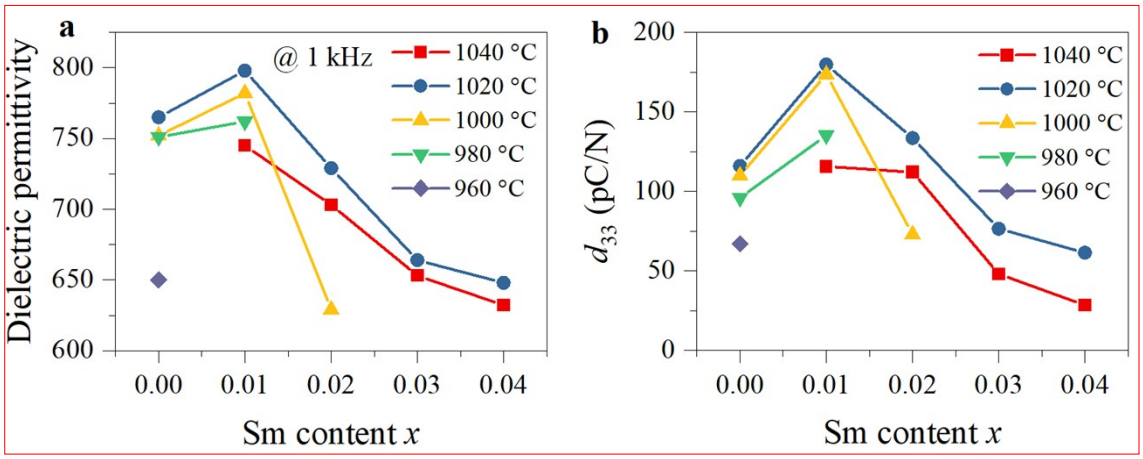

Fig. S3 Dielectric and piezoelectric properties of the $0.7BiFeO_3$-$0.3Ba_{1-x}Sm_xTiO_3$ ceramics at various sintering temperature.

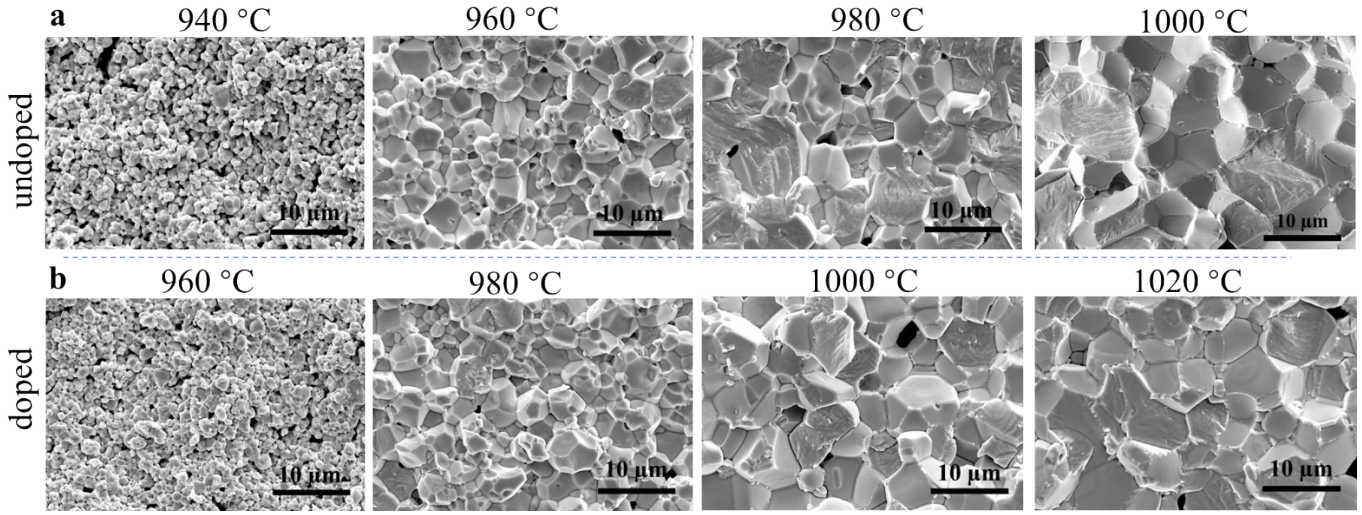

Fig. S4 Cross-sectional morphology of the undoped (**a**) and doped (**b**) ceramics observed by scanning electron microscopy. Sintering temperature varied from 940 °C to 1000 °C for undoped ceramic, while varied from 960 °C to 1020 °C for doped ceramic. Under same sintering temperature, grain size of doped ceramic is smaller than that of undoped one.

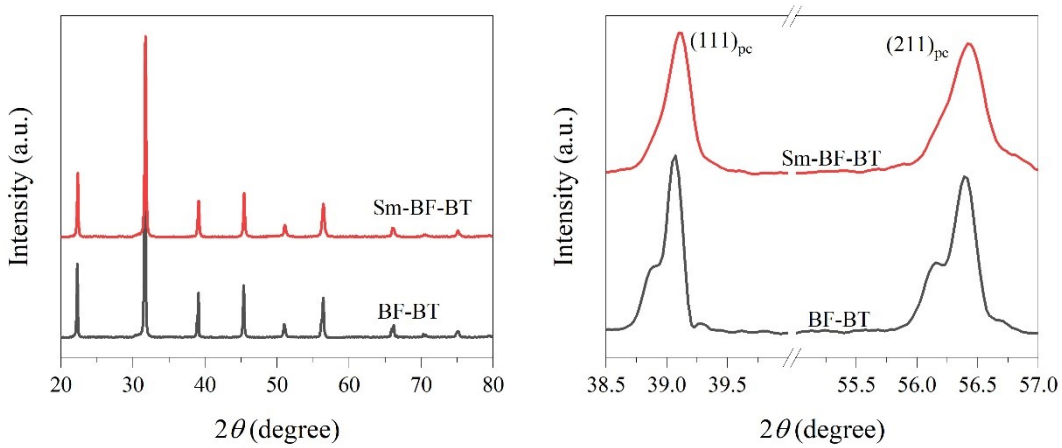

Fig. S5 X-ray diffraction patterns of the ceramic powder at room temperature.

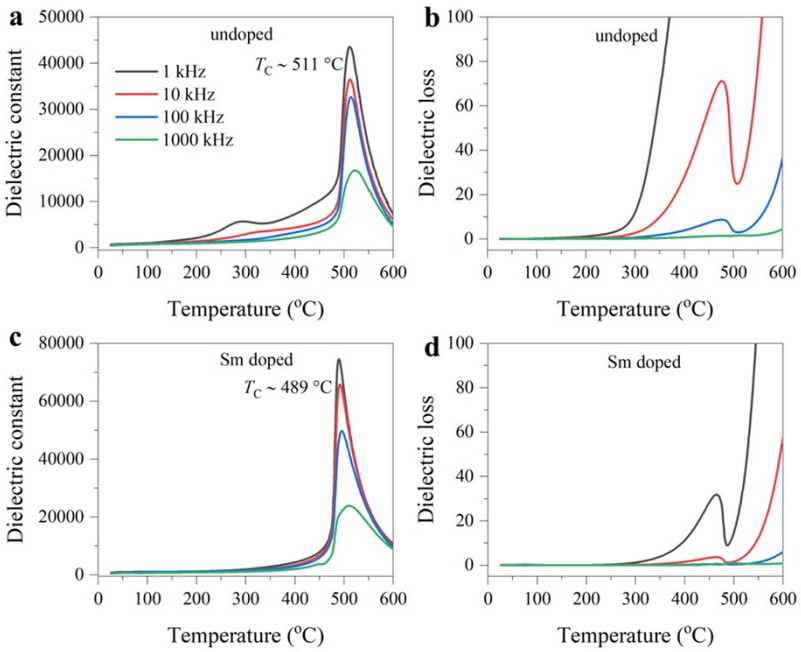

Fig. S6 The temperature-dependent dielectric constant and loss of the undoped (**a**, **b**) and doped (**c**, **d**) samples at different measuring frequencies.

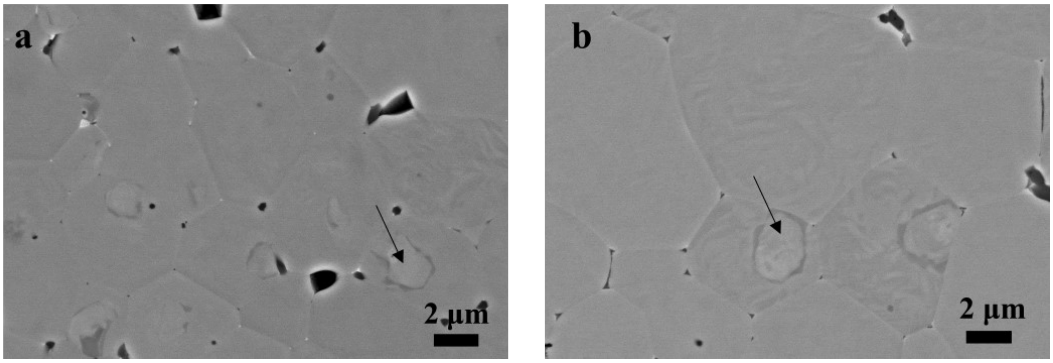

Fig. S7 The morphology of the polished surface for the undoped (a) and Sm-doped (b) BF-BT ceramic observed by scanning electron microscopy with a backscattered electron detector.

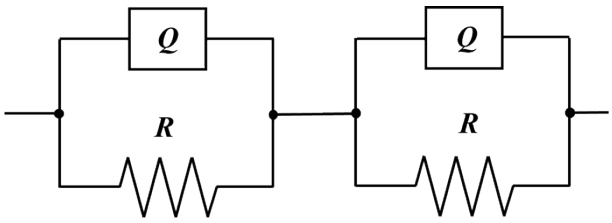

Fig. S8. Equivalent circuits model consisting of two parallel RQ elements connected in series.

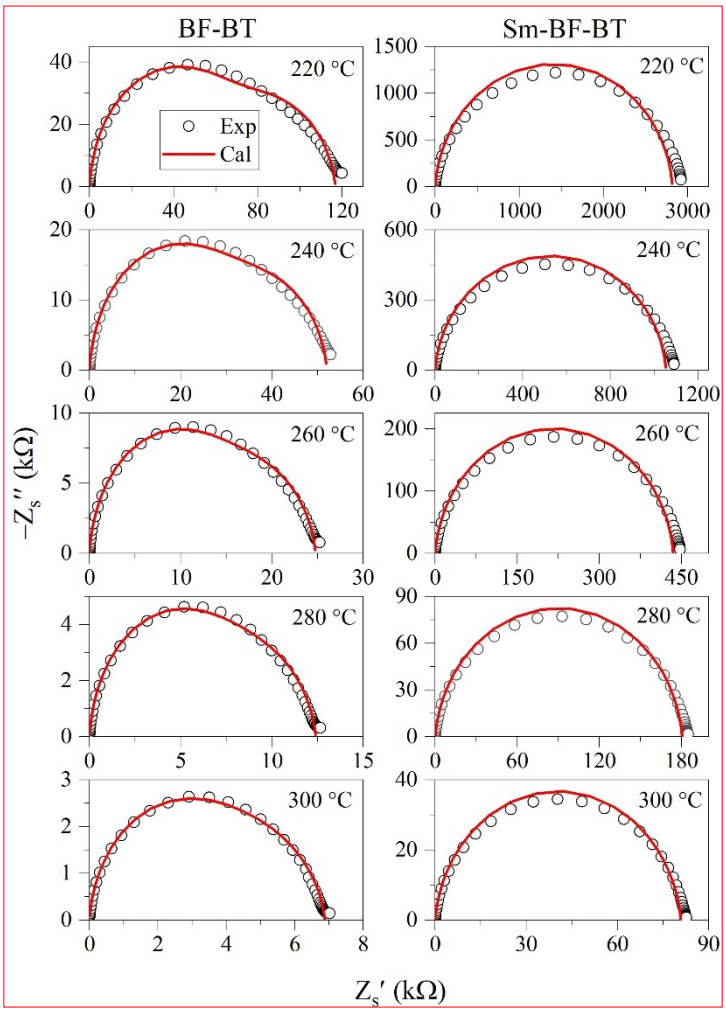

Fig. S9. Complex impedance plane plots of measured (open circles) and fitted (line) data for several temperatures: (a) the BF-BT ceramic, (b) the Sm doped BF-BT ceramic.

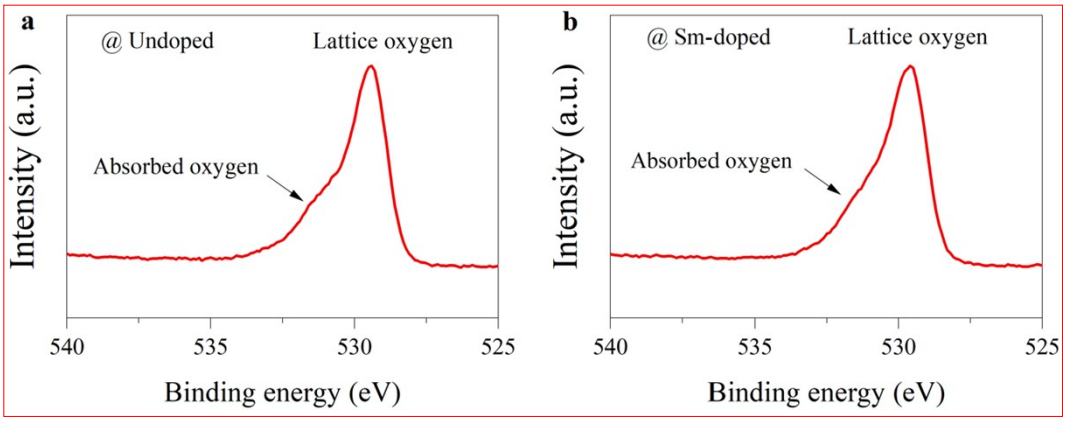

Fig. S10. X-ray photoelectron spectroscopy (XPS) of O 1s for the undoped (a) and doped (b) samples.

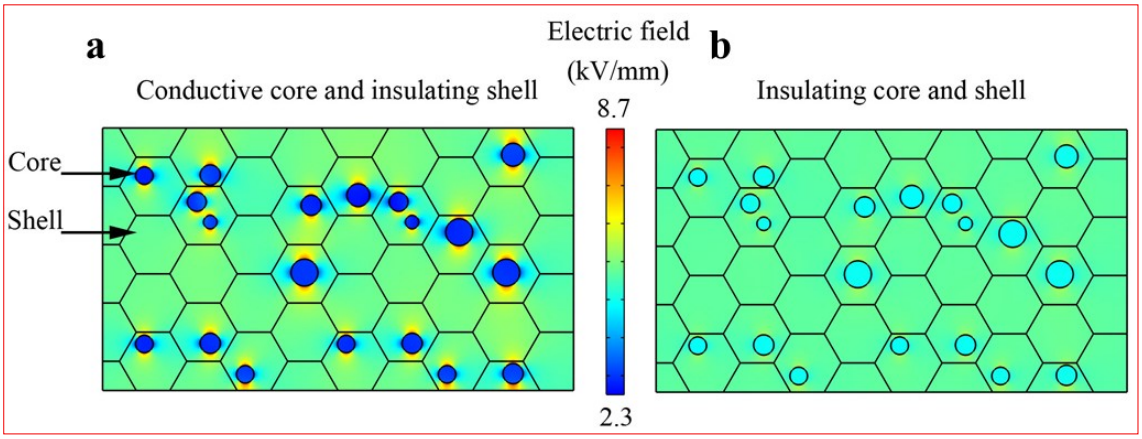

Fig. S11 The electric field distribution for the electrically heterogeneous (**a**) and homogeneous (**b**) dielectrics simulated by the COMSOL Multiphysics. For the former, the conductivity of the core is much higher than the shell. For the latter, their conductivities are almost the same.

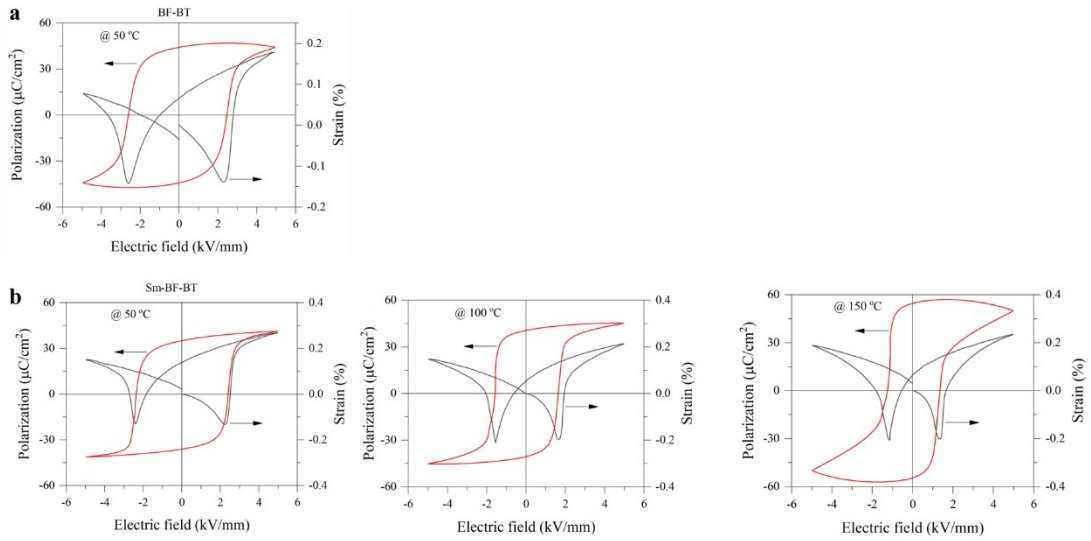

Fig. S12 The polarization and electric field-induced strain loops of the undoped (**a**) and doped (**b**) BF-BT samples at various temperature.

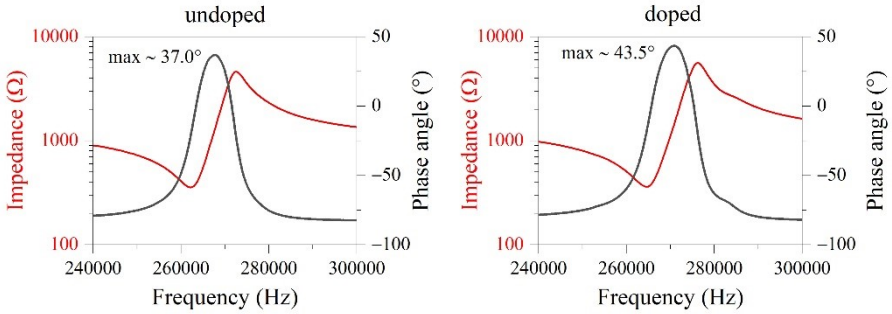

Fig. S13 The impedances and phase angles of the undoped (**a**) and doped (**b**) BF-BT samples near their resonance frequencies.

Table S1 Refined structural parameters and agreement factors for the undoped and Sm doped BF-BT ceramics.

Sample	Space group	*a* (Å)	*c* (Å)	Cell Volume (Å^3)	Phase fraction (%)	R_{wp} (%)	χ^2
BF-BT	*R*3*c*	5.6495	13.8887	383.893	46	11.2	4.01
	$Pm\bar{3}m$	3.9881	—	63.432	54		
Sm-BF-BT	*R*3*c*	5.6268	13.9020	381.180	25	10.5	3.86
	$Pm\bar{3}m$	3.9933	—	63.678	75		

Table S2 The key parameter in COMSOL assumption models.

Material	Region	Dielectric permittivity	Conductivity ($\times 10^{-9}$ S m^{-1})
undoped	Shell	1400	1.6
	Core	400	5.0
Sm-doped	Shell	1200	1.5
	Core	700	1.7